Proc. of the 8th International Symposium on Geotechnical Safety and Risk (ISGSR)
Edited by Jinsong Huang, D.V. Griffiths, Shui-Hua Jiang, Anna Giacomini and Richard Kelly
 Published by Research Publishing, Singapore.
doi: 10.3850/978-981-18-5182-7_03-016-cd

ISGSR 2022

The Effectiveness of Spatial Interpolation of Sparse PCPT Data to Optimise Offshore Design

Michael O'Neill[1], Fraser Bransby[1] and Phil Watson[1]

[1]ARC Research Hub for Transforming energy Infrastructure through Digital Engineering (TIDE), Oceans Graduate School, The University of Western Australia, M053, Perth WA 6009 Australia.
E-mail: michael.oneill@uwa.edu.au
fraser.bransby@uwa.edu.au
phillip.watson@uwa.edu.au

Abstract: The geotechnical data available to offshore infrastructure designers is invariably sparse, necessitating the use of engineering judgement in deriving (or estimating) soil design properties at untested (unsampled) locations. This task becomes more challenging when dealing with seabeds having a complex (layered) soil stratigraphy. Recent (and growing) interest in data-centric methods and their application to sparse datasets has seen progress in the spatial interpolation/extrapolation of geotechnical data using statistical and analytical approaches. This paper describes a case study involving one such approach where Bayesian Compressive Sensing and Markov Chain Monte Carlo methods are applied to a sparse two-dimensional PCPT dataset obtained from an offshore deep-water location comprising a layered (non-uniform) seabed. Results from the study are used to examine the ability of the considered approach in addressing soil variability and uncertainty in PCPT parameter estimation and highlights the difficulty in applying such approaches to complicated real-world settings.

Keywords: Site characterisation; offshore foundations; uncertainty; spatial variability.

1 Introduction

In an offshore project, the piezocone penetrometer test (PCPT) is a common industry-accepted approach for characterising seabed sediments. The number of PCPTs performed as part of a site investigation either for an offshore development (which may comprise fixed or floating wind turbines or platforms, or fixed subsea structures) or along a pipeline or cable alignment is often limited by technical and operational constraints, as well as high costs – and the amount of data available to support design is almost always sparse. In addition, layouts or alignments may change after the investigation and individual PCPT locations may no longer align with key infrastructure. Therefore, foundation designers are often required to employ engineering judgement in using the available data (at 'sampled' locations) to select design PCPT profiles, and by extension engineering parameters, at untested (or 'unsampled') locations. The consequential risk to offshore infrastructure fabrication, installation and performance can be significant.

Ongoing improvement in off-the-shelf computational capability has seen growing interest in the application of data-centric methods to analyse and use measured data, with recent publications describing methods for interpolation (and extrapolation) of data via statistical and analytical approaches. One particular method proposed by Zhao et al. (2020) combines Bayesian compressive sampling (BCS) with Markov Chain-Monte Carlo techniques in a two-dimensional (2D) spatial framework, allowing for a more formal treatment of uncertainty in the estimation of parameters at unsampled locations.

Building on a previous study that examined the application of this particular 'BCS' method to select geotechnical design properties and the potential impact on foundation sizing (O'Neill et al. (2022)), the same method is applied in this paper to a new sparse 2D PCPT dataset obtained from an offshore location – but where the seabed has a complex (layered) soil stratigraphy. A series of example analyses are used to highlight the manner in which the method incorporates uncertainty in estimating PCPT profiles at unsampled locations. Through examination of the analysis results, this paper identifies strengths and weaknesses of statistical methods and their ability to mitigate risks associated with uncertainty in soil parameter estimation. Noting that a future goal of this work is to compare the BCS method with other existing advanced statistical approaches and/or develop new approaches, the objective of the paper is to highlight the challenges faced by foundation designers in applying advanced statistical data-centric approaches to complex real-world settings.

2 PCPT Data

2.1 Overview

The field PCPT data considered in this study were gathered at a deep-water site situated offshore north-west Australia. Figure 1 presents a layout of the survey area showing the locations of the five PCPTs (PCPT1 to PCPT5)

considered in this study. The tests were performed at near-regular intervals along the survey line, with a horizontal distance (x, where PCPT1 is located at x = 0 m) of 142 m separating the outer PCPTs. Each test was performed at a constant rate of penetration (0.02 m/s), with data recorded continuously at regular depth increments (Δz) of 0.02 m. A geotechnical laboratory testing program was performed on soil samples obtained from the site. Interpretation of the field and laboratory data indicated the sediments across the site comprise high plasticity carbonate muddy silts and silty muds, with occasional localised thin lenses of carbonate silty/muddy sands.

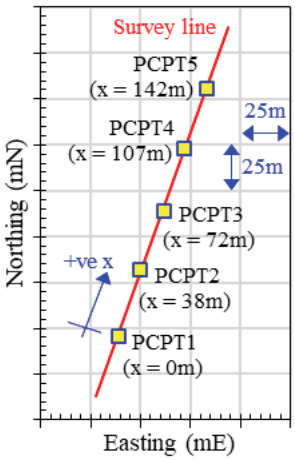

Figure 1. PCPT locations.

Figure 2 shows profiles of the field-measured (sampled) cone resistance ($q_{c\text{-}f}$) and pore pressure ($u_{2\text{-}f}$) versus depth below the mudline (z) obtained at the PCPT1 to PCPT5 locations down to 20 m depth, together with the corresponding inferred profiles of measured net cone resistance ($q_{net\text{-}f} = q_{c\text{-}f} + u_{2\text{-}f}\,[1 - \alpha] - \sigma_{vo}$, where α = cone tip area ratio and σ_{vo} = total in situ vertical stress) and excess pore pressure ratio ($B_{q\text{-}f} = [u_{2\text{-}f} - \gamma_w\, z] / q_{net\text{-}f}$, where γ_w = unit weight of seawater). The data indicate that between the mudline and approximately 8 m depth $q_{net\text{-}f}$ and $B_{q\text{-}f}$ are reasonably uniform across the survey line (i.e. as x varies), with relatively lower $q_{net\text{-}f}$ and higher $B_{q\text{-}f}$ values inferring the presence of silts and carbonate muds. Extending beyond around 8 m depth $q_{net\text{-}f}$ and $B_{q\text{-}f}$ show significant variability, with abrupt increases in $q_{net\text{-}f}$ and corresponding reductions in $B_{q\text{-}f}$ (and vice versa) at varying depths signifying an overall increased sand fraction and the presence of silty/muddy sand lenses. Notably, there is no easily discernable trend in the depth intervals of these various soil units (layers) with respect to horizontal position along the seabed.

2.2 Sampled PCPT data scenarios

For this study three different 'sampled data' scenarios were considered as input to the BCS analysis:

- Run 1 considered $q_{c\text{-}f}$ and $u_{2\text{-}f}$ from all five PCPTs.
- Run 2 considered $q_{c\text{-}f}$ and $u_{2\text{-}f}$ from PCPT1/3/5 (three PCPTs), excluding PCPT2 (x = 38 m) and PCPT 4 (x = 107 m).
- Run 3 considered $q_{c\text{-}f}$ and $u_{2\text{-}f}$ from PCPT2/4 (two PCPTs), excluding PCPT1 (x = 0 m), PCPT 3 (x = 72 m) and PCPT 5 (x = 142 m).

Note for Run 2 and Run 3 data from the excluded PCPTs were assumed to be unseen (unsampled).

2.3 Standard assessment of PCPT data for design

A 'standard' (traditional) approach to assessing PCPT data as part of the geotechnical design of subsea infrastructure often entails the identification and generation of simplified representative profiles of the data versus depth. The nature of a given profile (relative to the data) is generally dependent on the type of design assessment the profile will be applied to. For foundation capacity (stability) a 'low estimate' (LE) of the inferred soil strength would be considered, for foundation installation (e.g. mudmat skirt penetration, suction anchor installation) a 'high estimate' (HE) of the inferred soil strength would be used, while for serviceability requirements (e.g. foundation settlement) a 'mean' (or 'best-fit') of the inferred soil strength (or stiffness) would be more appropriate. The LE

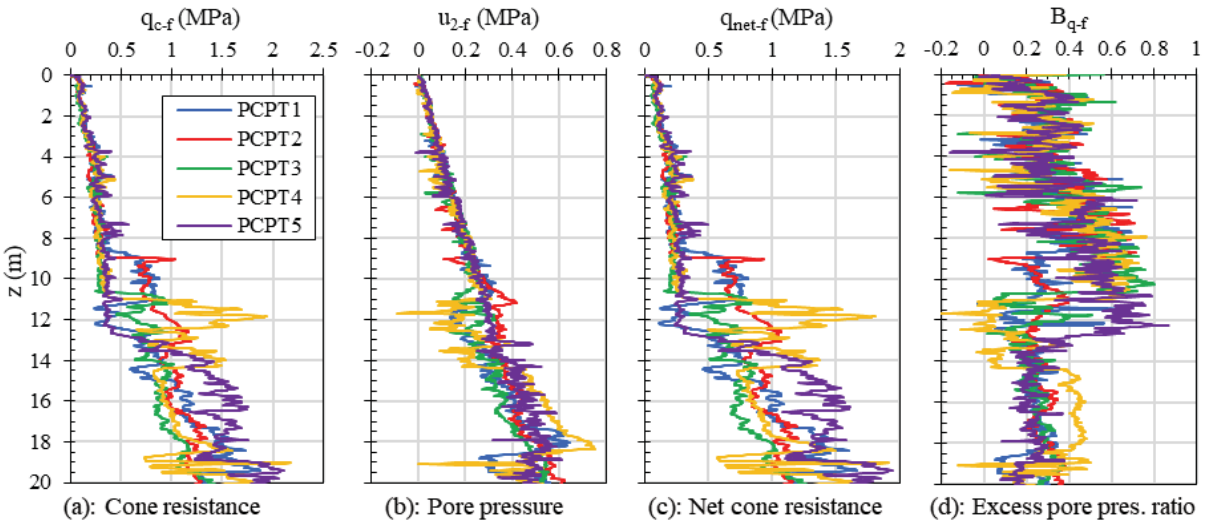

Figure 2. PCPT measured cone resistance, pore pressure, net cone resistance & excess pore pressure ratio versus depth.

and HE profiles are often selected based on corresponding quantile regression (QR; e.g. Uzielli et al., 2019) or percentile profiles of the data. The point to note is in general terms these simple design profiles usually apply across the full survey area (or line) and are independent of horizontal location (in this case represented by x).

An example of the standard PCPT data assessment approach is presented on Figure 3a, which shows the $q_{net\text{-}f}$ versus depth profiles for the Run 1 sampled data scenario (i.e. all five PCPTs). Included on the figure is the corresponding proposed piecewise-linear 'Design-Mean' net cone resistance ($q_{net\text{-}dm}$) profile, which was generated by minimising the 'sum-of-squares' of the difference between the mean of the natural log values of $q_{net\text{-}f}$ at each depth interval and the natural log of the corresponding Design-Mean value. Natural log values were adopted since log-normal distributions are recognised as a reasonable statistical model for soil (and geological) properties (Lacasse 1994; Griffiths et al. 2009) and ensure non-negative estimated net cone resistance values in the BCS analysis (see Section 3). Figure 3a also shows proposed piecewise-linear design bounds to the $q_{net\text{-}f}$ data, with the LE represented by a nominal 10th quantile regression (QR10) profile ($q_{net\text{-}dqr10}$) and the HE represented by a nominal 90th quantile regression (QR90) profile ($q_{net\text{-}dqr90}$). Note that for this study the Design-Mean, QR10 and QR90 profiles were each limited to a nominal maximum of twelve 'layers' across the 20 m depth interval.

2.4 Variability of PCPT data

In addition to the range of measured net cone resistance inferred by the design QR10-QR90 profiles, the variability of $q_{net\text{-}f}$ across the site may also be expressed in terms of the coefficient of variation (COV) defined as the ratio of the standard deviation versus mean of the data. The top of Figure 3b shows a histogram of the same (complete; $z \leq 20$ m) Run 1 dataset in terms of the natural log of [$q_{net\text{-}f}$ / $q_{net\text{-}dm}$], together with the corresponding normal distribution (ND) of the data which has a COV of 0.32. Compared to the ND the data has a slightly more pronounced peak about the mean. It is noted the kurtosis value of the (full) Run 1 dataset equal to 4.7 is slightly higher than the ND 'reference' value of 3.0, which in turn implies a greater proportion of the variance in Ln [$q_{net\text{-}f}$ / $q_{net\text{-}dm}$] is the result of infrequent large deviations rather than frequent small deviations (Westfall, 2014). Noting the earlier observation regarding the greater variability in $q_{net\text{-}f}$ beyond 8 m depth, Figure 3b also shows separate Run 1 dataset histograms for $z \leq 8$ m (COV = 0.19) and $z > 8$ m (COV = 0.38).

For reference, considering the complete ($z \leq 20$ m) Run 2 and Run 3 datasets the corresponding ND fits to Ln [$q_{net\text{-}f}$ / $q_{net\text{-}dm}$] give COV values of 0.29 and 0.22 respectively. It is interesting to note the COV decreases as the number of PCPTs (i.e. amount of available $q_{net\text{-}f}$) also decreases. For the situation where the seabed comprised a single soil unit (i.e. no layering) it would be expected the COV would not change discernibly as the number of PCPTs decreased. However, in this scenario where various soil units (layers) were detected at different (non-uniform) depth intervals across the survey line, as the number of PCPTs increases the mismatch between the soil layer boundaries also increases, which is reflected by the increasing COV.

3 BCS Analysis of PCPT Data

The BCS approach as proposed by Zhao et al. (2020) for interpolating (and extrapolating) sparse geotechnical data allows for the incorporation of uncertainty in the estimation of geotechnical properties at unsampled locations. The method is simple to code and implement, and the algorithm is computationally efficient. In addition, the approach is able to accommodate 'non-stationary' data – that is, soil stratigraphies comprising multiple soil types (units) with spatially varying statistical properties – which in a 'real-world' context is advantageous over other approaches that can only consider 'stationary' data (where the statistical properties of the soil do not change).

3.1 Consideration of PCPT measurement uncertainty

The BCS analyses undertaken for this study included an estimate of measurement uncertainty associated with the PCPT $q_{c\text{-}f}$ and $u_{2\text{-}f}$ data using the method proposed by Peuchen and Terwindt (2015). Consideration was given to uncertainty stemming from force and pressure sensor measurements, geometry errors, ambient and transient temperature and pressure effects and measurement offsets (relative to the mudline). The estimated total (combined) uncertainty was assumed to be normally distributed about the measured (mean) $q_{c\text{-}f}$ or $u_{2\text{-}f}$ value with a standard deviation expressed as a function of $q_{c\text{-}f}$ or $u_{2\text{-}f}$. Uncertainty associated with the measurement or application of other analysis parameters, including the cone tip area ratio (α), total in situ vertical stress (σ_{vo}) and unit weight of seawater (γ_w), has not been accounted for at this time.

3.2 BCS analysis parameters

A pair of 2D BCS analyses (one considering each of $q_{c\text{-}f}$ and $u_{2\text{-}f}$ as input data) were undertaken for each of the three sampled data scenarios outlined in Section 2.2. As mentioned previously, an objective of the study was to apply the BCS method to the interpolation (within the PCPT spatial envelope) and extrapolation (outside the PCPT

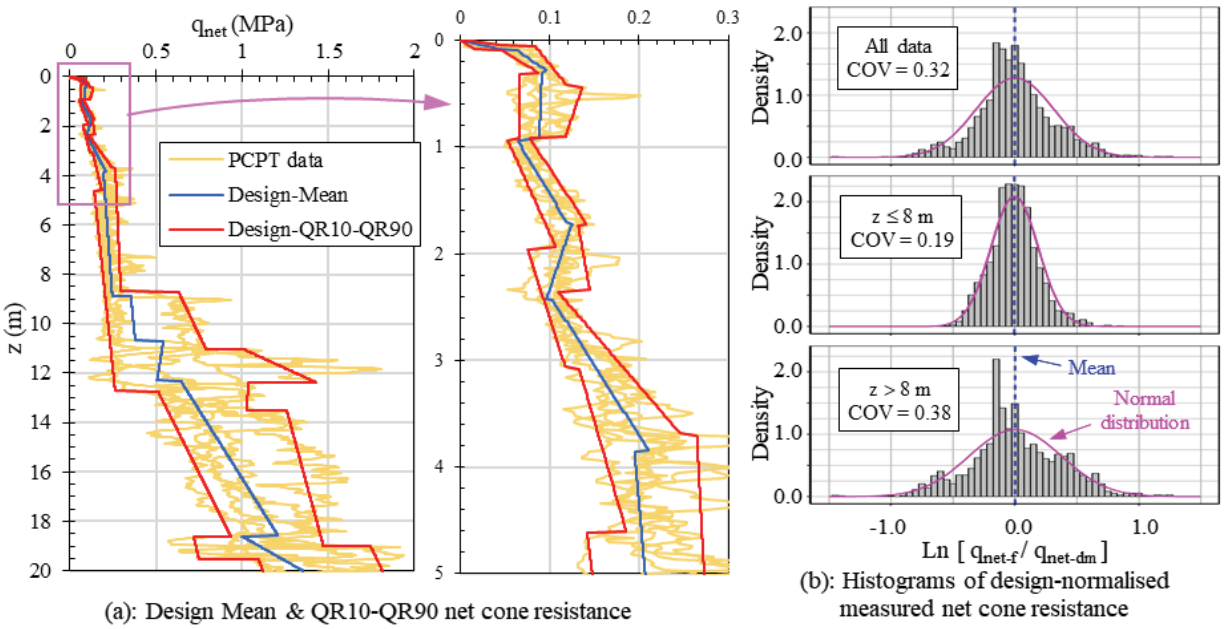

(a): Design Mean & QR10-QR90 net cone resistance

(b): Histograms of design-normalised measured net cone resistance

Figure 3. Run 1 (×5 PCPT) –design net cone resistance versus depth & histograms of design-normalised measured net cone resistance.

spatial envelope) of measured data; one reason for extrapolating beyond the outboard PCPTs is to allow for the subsequent 2D analysis of foundations centred at one of these outboard PCPTs. Noting the near-regular horizontal (x) spacing of PCPTs along the survey line for each sampled data scenario (i.e. x-spacing range of 34 m – 38 m for Run 1, and 69 m – 72 m for Run 2 and Run 3), each BCS analysis extended horizontally across the survey line and beyond the outboard PCPT locations a distance of approximately one half of the corresponding PCPT x-spacing. Hence, the Run 1 analyses extended from x = -17 m to x = 159 m, the Run 2 analyses extended from x = -35 m to x = 177 m, and the Run 3 analyses extended from x = 0 m to x = 142 m. All analyses extended vertically from the mudline to 20 m depth and used uniform horizontal and vertical spatial increments of $\Delta x = 1.0$ m and $\Delta z = 0.02$ m respectively. The BCS analyses of $q_{c\text{-}f}$ adopted the natural log values of the input data, while the analyses of $u_{2\text{-}f}$ adopted standard (non-log) input values.

Each BCS analysis comprised a total of 50,500 iterations. Prior to commencing the analysis, a set of random normally distributed measurement uncertainty values was added to the input $q_{c\text{-}f}$ or $u_{2\text{-}f}$ data. Upon commencement each analysis underwent an initial period of numerical stabilisation, and hence the results from the initial 500 iterations were discarded. In order to ensure the final results were statistically independent, the results from every 100th iteration (from the remaining 50,000 iterations) were saved while those from the other iterations were also discarded. Furthermore, immediately after a set of analysis results was saved and prior to commencement of the next 100 iterations, a new set of random normally distributed measurement uncertainty values was added to the input $q_{c\text{-}f}$-$u_{2\text{-}f}$ data. Therefore, upon completion each BCS analysis produced 500 independent 'sets' of estimated cone resistance ($q_{c\text{-}be}$) or pore pressure ($u_{2\text{-}be}$) across the full corresponding z-x cross-section.

3.3 BCS analysis results – net cone resistance

Results obtained from the Run 1 (five PCPT) BCS analyses considering $q_{c\text{-}f}$ and $u_{2\text{-}f}$ are presented on Figure 4 as example profiles of the estimated net cone resistance ($q_{net\text{-}be}$, 'BCS-Estimate', calculated as $q_{net\text{-}be} = q_{c\text{-}be} + u_{2\text{-}be}\,[1 - \alpha] - \sigma_{vo}$) versus depth (z) at x = 38 m (coincident with PCPT2), 55 m (midway between PCPT2 and PCPT3), 72 m (coincident with PCPT3), 90 m (midway between PCPT3 and PCPT4) and 107 m (coincident with PCPT4). The example $q_{net\text{-}be}$ profiles correspond to the 50th, 150th, 250th, 350th and 450th result sets (out of a total of 500 sets) output from the analyses. Included on the plots are the corresponding mean ($q_{net\text{-}bm}$, 'BCS-Mean') and 10th and 90th percentile ($q_{net\text{-}bp10\text{-}bp90}$, 'BCS-P10-P90') estimated net cone resistance profiles calculated from the 500 result sets, while Figure 4a, Figure 4c and Figure 4e also show the respective PCPT $q_{net\text{-}f}$ profiles. At the PCPT locations (x = 38 m, 72 m and 107 m) q_{net} is measured (known; i.e. $q_{net\text{-}f}$), and hence the corresponding estimated values are considered to be reliable – as evident by the similar $q_{net\text{-}be}$, $q_{net\text{-}bm}$, $q_{net\text{-}bp10\text{-}bp90}$ and $q_{net\text{-}f}$ profiles. Note the small (but non-zero) range in $q_{net\text{-}be}$ inferred by the $q_{net\text{-}bp10\text{-}bp90}$ profiles at the PCPTs originates from the inclusion of PCPT measurement uncertainty. Conversely, at x = 55 m (Figure 4b) and x = 90 m (Figure 4d) no information on $q_{net\text{-}f}$ is available, and therefore $q_{net\text{-}be}$ is considered to be less reliable (more uncertain) – as evident by the wider $q_{net\text{-}be}$ range inferred by the $q_{net\text{-}bp10\text{-}bp90}$ profiles.

Further results obtained from the Run 1 BCS analyses are presented on Figure 5a and Figure 5b as z-x heat maps showing the mean ($q_{net\text{-}bm}$) and COV ($q_{net\text{-}bcov}$) of the estimated net cone resistance respectively (where

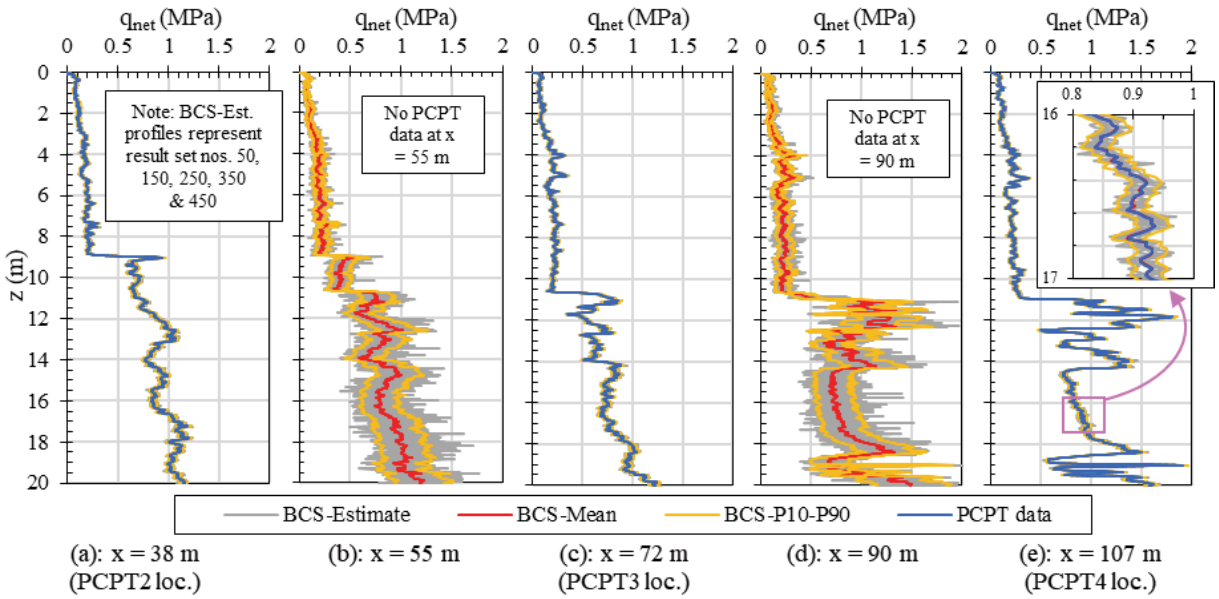

Figure 4. Run 1 (×5 PCPT) BCS analysis results – comparison of estimated, mean estimated, P10-P90 estimated & measured net cone resistance versus depth.

$q_{net\text{-}bcov}$ = [$q_{net\text{-}bsd}$ / $q_{net\text{-}bm}$] and $q_{net\text{-}bsd}$ is the standard deviation of $q_{net\text{-}be}$). The PCPT locations are indicated on the maps. The $q_{net\text{-}bm}$ map in particular provides an informative illustration of the overall soil unit structure across the survey line inferred from the full (five PCPT) $q_{net\text{-}f}$ dataset presented on Figure 2c. Additionally, the results presented on the $q_{net\text{-}bcov}$ map are consistent with those shown on Figure 4, in that the 'variability-reliability' mix of the estimated net cone resistance values is low-high at sampled locations and relatively higher-lower at unsampled locations. It can also be seen that $q_{net\text{-}bcov}$ increases as the horizontal distance (x) from the nearest PCPT (sampled) location also increases.

Similar z-x heat maps showing $q_{net\text{-}bm}$ and $q_{net\text{-}bcov}$ determined from the BCS analyses are presented on Figure 5c and Figure 5d respectively for Run 2 (three PCPTs) and on Figure 5e and Figure 5f respectively for Run 3 (two PCPTs). Note all maps included on Figure 5 use consistent axes and scales to allow direct comparison. The $q_{net\text{-}bm}$ maps highlight the change in the inferred soil unit structure across the survey line that occurs as the number of PCPTs (volume of available sampled data $q_{net\text{-}f}$) decreases (and the spacing between PCPTs increases); the overall reduction in the fidelity of $q_{net\text{-}bm}$ is also easily discernable. Correspondingly, the $q_{net\text{-}bcov}$ maps highlight the increasing variability in $q_{net\text{-}be}$ with decreasing $q_{net\text{-}f}$ volume and increasing PCPT spacing.

Useful insight into the predictive functionality of the BCS method and overall structure of the analysis results is presented on Figure 6, which shows profiles of the Run 1, Run 2 and Run 3 BCS mean and 10^{th}-90^{th} percentile estimated net cone resistance ($q_{net\text{-}bm}$ and $q_{net\text{-}bp10\text{-}bp90}$ respectively) versus horizontal distance along the survey line (x) at nominal depths below mudline (z) of 5 m and 15 m. The PCPT locations are indicated on the plots. It can be seen on the figure that the $q_{net\text{-}bm}$ and $q_{net\text{-}bp10\text{-}bp90}$ profiles essentially represent near-smooth continuous functions of x. For each sampled data scenario the known $q_{net\text{-}f}$ values at the respective PCPT locations effectively constrain the range of estimated $q_{net\text{-}be}$., with the small amount of variability in $q_{net\text{-}be}$ at the PCPTs stemming from PCPT measurement uncertainty. Conversely, with increasing horizontal distance from the nearest PCPT location the $q_{net\text{-}bp10\text{-}bp90}$ range widens, reflecting increasing variability in $q_{net\text{-}be}$. Figure 6 also highlights at each of the selected depths the interaction between the relative $q_{net\text{-}f}$ data values, and how differences between spatially adjacent $q_{net\text{-}f}$ points influences the shape and form (trend) of the $q_{net\text{-}bm}$ and $q_{net\text{-}bp10\text{-}bp90}$ profiles.

A further demonstration of the Run 1, Run 2 and Run 3 BCS analysis results structure is presented on Figure 7 as profiles of the COV of the estimated net cone resistance ($q_{net\text{-}bcov}$) versus horizontal location (x) at z = 5 m and 15 m. The PCPT locations are again highlighted on the figure. The results show that for a given sampled data scenario (i.e. Run 1, Run 2 or Run 3) and value of x the variation of $q_{net\text{-}bcov}$ with z is generally small. Also note the small $q_{net\text{-}bcov}$ values (in the range of 0.02 –0.06) at the PCPTs which represent PCPT measurement uncertainty. In addition, the figure captures the outcome of two competing and opposing variability effects, namely an increase in the number of PCPTs leading to an increase in the COV of Ln [$q_{net\text{-}f}$ / $q_{net\text{-}dm}$] (reflecting the increasing mismatch between the soil layer boundaries across the site; see Section 2.4) and a decrease in the number of PCPTs (i.e. reduced amount of input $q_{net\text{-}f}$) leading to an overall increased level of uncertainty in $q_{net\text{-}be}$. In broad terms it can be seen that as the number of PCPTs decreases the maximum $q_{net\text{-}bcov}$ occurring midway between PCPT locations tends to increase.

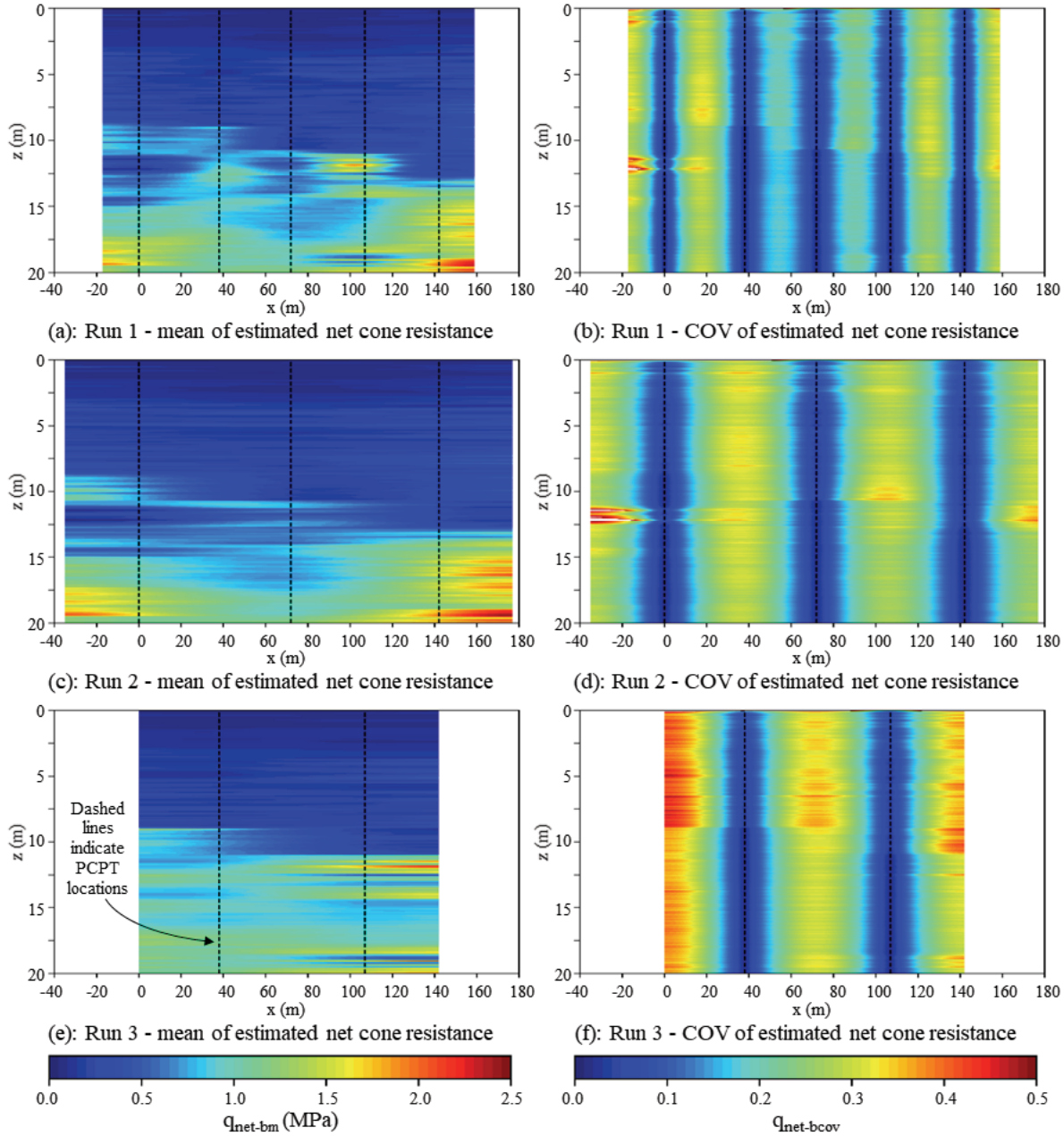

Figure 5. BCS analysis results – heat maps of mean and COV of estimated net cone resistance.

An assessment of the performance of the BCS method in predicting q_{net} at unsampled locations may be obtained by interrogating the Run 2 and Run 3 BCS analysis results at the excluded PCPT locations. Figure 8a shows the q_{net-f} profile for PCPT2 (x = 38 m), together with the mean and P10-P90 estimated profiles from the Run 2 BCS analyses at x = 38 m. In this scenario where the PCPT2 q_{c-f} and u_{2-f} were excluded from the BCS analysis input, we can quantify the performance of the BCS method in predicting the measured q_{net-f}. The mean estimated (q_{net-bm}) profile shows reasonable agreement with q_{net-f} over the upper 8.5 m and beyond 14.0 m depth, while between 8.5 m 14.0 m depth there is some mismatch. Comparing the q_{net-bm} and q_{net-f} profiles over the upper 8.0 m of relatively uniform soil, the Run 2 average normalised prediction error for PCPT2 (expressed as the average value of abs[(q_{net-bm} – q_{net-f}) / q_{net-f}] over the specified depth interval) was 19.9 %; across the full depth interval considered in the analysis (mudline to z = 20 m) the q_{net-f} prediction error increased only slightly to 22.5 %. The prediction error values are listed on Figure 8a.

Similar sets of results are presented on Figure 8b for Run 2-PCPT4, Figure 8c for Run 3-PCPT1, Figure 8d for Run 3-PCPT3 and Figure 8e for Run 3-PCPT5. The BCS method was reasonably consistent at predicting q_{net-f} over the upper 8 m (uniform soil), with an average normalised prediction error ranging between 18.2 % – 19.9 % for Run 2 and 18.0 % – 22.5 % for Run 3. Considering the full 20 m depth interval the prediction error for Run 2 (three PCPTs) increased slightly to 22.5 % – 23.3 %, while for Run 3 (two PCPTs) the prediction error increased significantly to 36.1 % – 57.7 %. In several cases the BCS analysis prediction of the transition from

weaker to stronger soil (and vice versa) was incorrect; with specific reference to Figure 8e it can be clearly seen that the Run 3 prediction of the weaker-to-stronger soil transition situated at around 13 m depth was off by around 2 m. In general terms these results reflect the increasing difficulty in predicting the 'unseen' $q_{net\text{-}f}$ data that arises due to both the reduction in the volume of 'known' $q_{c\text{-}f}$ and $u_{2\text{-}f}$ data input to the BCS analysis and the greater variability of $q_{net\text{-}f}$ across the site at depths greater than 8 m. The results also highlight the need to incorporate other forms of geo-data (such as geophysical data) into the statistical analysis framework.

Additional insight into the performance of the BCS method in predicting $q_{net\text{-}f}$ may be obtained by determining what proportion of the measured data is less than (or exceeds) a given corresponding set of BCS-estimated percentile values (i.e. $q_{net\text{-}bp}$). For each combination of sampled data scenario and x location featured on Figure 8 and considering all values between the mudline and 20 m depth, Figure 9 shows the relationship between a given percentile of all BCS-analysis $q_{net\text{-}be}$ values (i.e. '$q_{net\text{-}bp}$ Percentile' ranging between 1 % – 99%) and the corresponding percentage of all $q_{net\text{-}f}$ values that don't exceed their corresponding $q_{net\text{-}bp}$-inferred values (i.e. '$q_{net\text{-}f}$ Non-Exceedance Percentile' ranging between 0 % – 100%). Included on Figure 9 is a unity line – values plotting below this line imply an excess of the measured data being greater than the given BCS percentile prediction (and vice versa). Across the full '$q_{net\text{-}bp}$ Percentile' range the Run 2-PCPT2 results indicate an excess of the PCPT2 data being greater than the Run 2 percentile predictions. Conversely, across the full percentile range the Run 3-PCPT3 results indicate an excess of the Run 3 percentile predictions being greater than the PCPT3 data. Also note the reduced (minimal) deviation of the Run 2-PCPT4 results from the unity line, suggesting the analysis performance in this case was better.

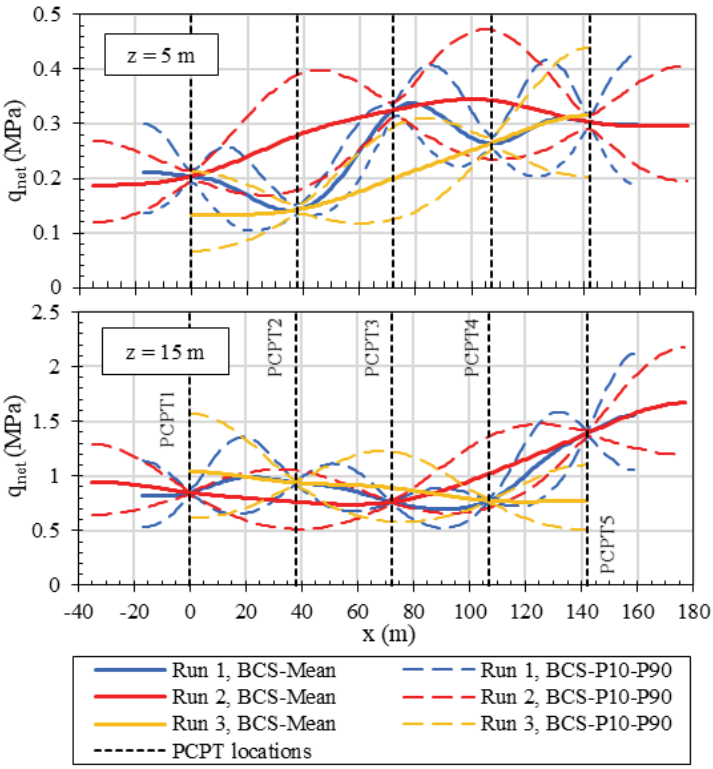

Figure 6. BCS analysis results – mean estimated & P10-P90 estimated net cone resistance versus horizontal distance.

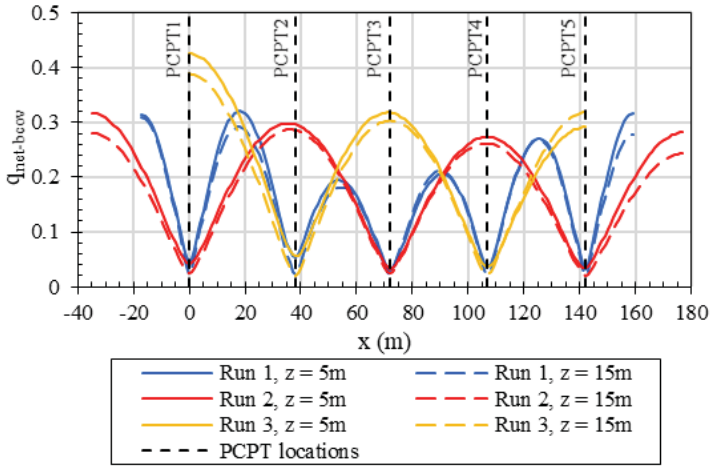

Figure 7. BCS analysis results – COV of estimated net cone resistance versus horizontal distance.

3.4 BCS analysis results – excess pore pressure ratio

The analyses discussed in Section 3.3 concerned the estimation of soil strength as represented by the net cone resistance. The BCS method is equally applicable to other useful geotechnical properties inferred from PCPT data, one of these being the excess pore pressure ratio (B_q) which reflects the drainage characteristics of the soil and is often used to categorise the soil into broad types (e.g. 'sand', 'silt', 'carbonate mud/clay', etc.).

As a demonstration of the estimation of B_q, Figure 10a shows a z-x heat map of the Run 1 mean estimated excess pore pressure ratio ($B_{q\text{-}bm}$) determined from the 500 sets of estimated excess pore pressure ratio ($B_{q\text{-}be}$, calculated as $B_{q\text{-}be} = [u_{2\text{-}be} - \gamma_w z] / q_{net\text{-}be}$). Similar z-x heat maps showing $B_{q\text{-}bm}$ are presented on Figure 10b for Run 2 and on Figure 10c for Run 3. The maps included on Figure 10 are presented using consistent axes and scales – the z-x axes are also consistent with those employed on Figure 5 (showing $q_{net\text{-}bm}$) to allow direct comparison. The $B_{q\text{-}bm}$ maps provide a useful high-level (and highly visual) representation of the estimated soil type across the

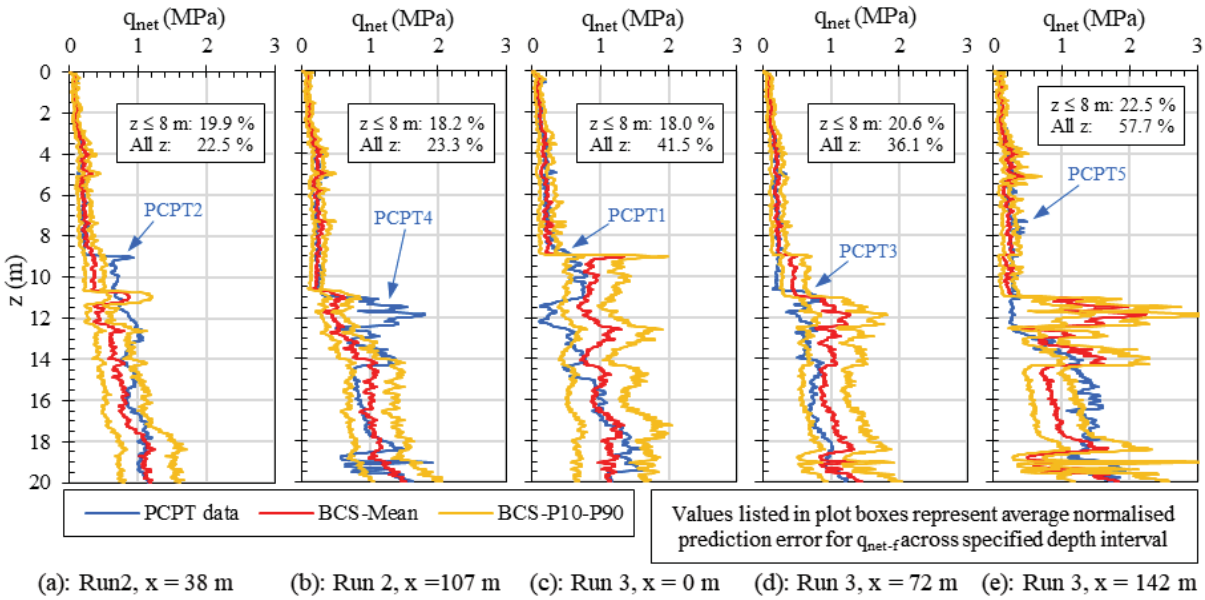

Figure 8. BCS analysis results – comparison of measured, mean estimated & P10-P90 estimated net cone resistance versus depth at PCPT locations.

Survey line considering the different sampled data scenarios, with $B_{q\text{-}bm} < \approx 0.05$ broadly indicating sand, $B_{q\text{-}bm} > \approx 0.6$ broadly indicating silt/carbonate mud/clay, and the intermediate $B_{q\text{-}bm}$ interval indicating the transition between sand and silt/mud/clay.

4 Conclusions

The study described in this paper provides a comprehensive demonstration of the application of an advanced data-led statistical approach to the interpolation and extrapolation of sparse 2D PCPT data obtained at an offshore location. Although the relatively small size of the dataset selected for the study limits the generalisability of the study findings, the complex (layered) and variable nature of the soil stratigraphy at the location makes the dataset ideal for providing the opportunity to properly assess the statistical method under 'real-world' conditions typically faced by foundation designers.

The study focused primarily on the estimation of net cone resistance and excess pore pressure ratio at unsampled (untested) locations across the 2D survey line of interest. An estimate of measurement uncertainty associated with the PCPT data was incorporated into the statistical analysis. In addition to assessing the full dataset, the study considered scenarios where the number of available PCPTs (and hence the volume of sampled data input to the BCS analysis) was reduced. Findings from the analysis highlighted changes in the inferred soil unit structure across the survey line that result from a reduction in the number of PCPTs (sampled data volume), and illustrated the corresponding overall reduction in the fidelity of the estimated net cone resistance.

Analysis results from the study captured the impact of opposing variability effects, namely an increase in the number of PCPTs leading to an increase in variability resulting from the increasing mismatch between soil layer boundaries across the site, and a decrease in the number of PCPTs leading to an increased level of uncertainty in the estimated soil properties. The results also showed that coupling of the estimated net cone resistance and excess pore pressure ratio provides a useful, high-level and highly visual representation of estimated soil type.

By excluding specific PCPTs from the BCS analysis input, the study also allowed for a direct statistical comparison of the

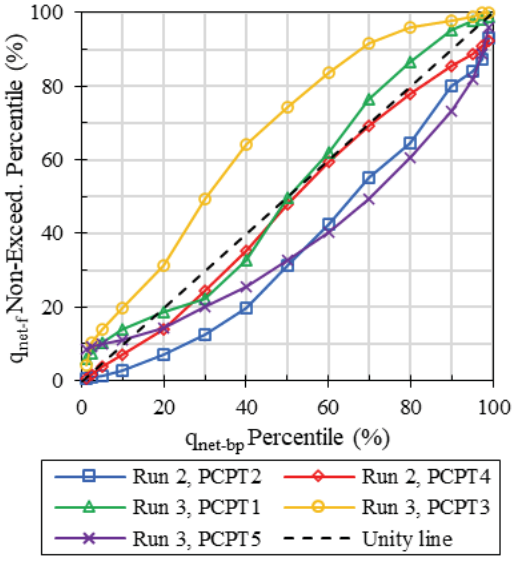

Figure 9. BCS analysis results – comparison of measured and estimated net cone resistance percentiles.

estimated net cone resistance obtained using the BCS approach with the actual measured (PCPT) values. This comparison highlighted the considerable challenge faced by statistical methods (and indeed foundation designers) – particularly in complex/variable soil stratigraphies – in predicting 'unknown' PCPT data at untested locations.

A key message of the study is that the predictive performance of advanced statistical approaches like the BCS method will still suffer from the relative sparseness typical of geotechnical datasets, particularly in real-world situations where the available data are invariably complex. Two important primary goals of future work on this topic will be to investigate other existing advanced statistical approaches and/or develop a new approach, and to incorporate 2D geophysical data into the statistical framework – such data is usually more 'plentiful' than PCPT data and can provide invaluable information on soil unit boundary alignments and potentially soil classification properties. Future work will also focus on acquiring larger datasets to permit a more thorough assessment of the performance of statistical approaches in predicting 'known-but-unseen' data, and on extending the approaches to a three-dimensional spatial framework.

Acknowledgments

This research is supported by the ARC ITRH for Transforming energy Infrastructure through Digital Engineering (TIDE, http://TIDE.edu.au) which is led by The University of Western Australia (UWA), delivered with The University of Wollongong and a number of Australian and international research partners, and funded by the Australian Research Council, INPEX Operations Australia, Shell Australia, Woodside Energy, Fugro Australia Marine, Wood Group Kenny Australia, RPS Group, Bureau Veritas and Lloyd's Register Global Technology (grant No. IH200100009). The second author holds the Fugro Chair in Geotechnics at UWA, whose support is gratefully acknowledged. The third author leads the Shell Chair in Offshore Engineering research team at UWA, which is supported by Shell Australia.

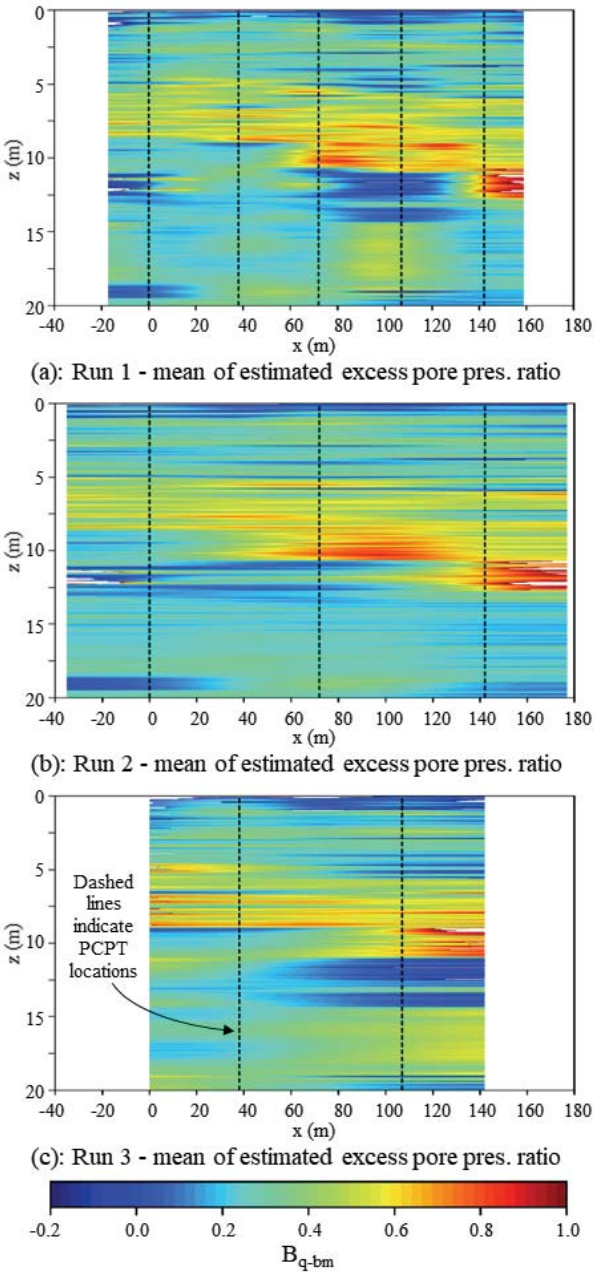

Figure 10. BCS analysis results – heat maps of mean estimated excess pore pressure ratio.

References

Griffiths, D.V., Huang, J. & Fenton, G.A. (2009). Influence of spatial variability on slope reliability using 2-D random fields. *Journal of Geotechnical and Geoenvironmental Engineering*, Vol. 135, No. 10, pp. 1367-1378.

Lacasse, S. (1994). Reliability & probabilistic methods. *Proc. 13th Int. Conf. Soil Mechanics & Foundation Engineering, New Delhi, India*, pp. 225–227.

O'Neill, M.P., Bransby, M.F., Doherty, J. & Watson, P. (2022). Spatial interpolation of sparse PCPT data to optimise infrastructure design. *Proc. 5th Int. Symp. Cone Penetration Testing (CPT'22), Bologna, Italy*.

Peuchen, J. & Terwindt, J. (2015). Measurement uncertainty of offshore Cone Penetration Tests. *Proc. 3rd Int. Symp. Frontiers in Offshore Geotechnics (ISFOG 2015)*, Vol. 1, pp. 1209-1214, https://www.proquest.com/docview/2115977051.

Uzielli, M., Zei, M. & Cassidy, M.J. (2019). Probabilistic assignment of design undrained shear strength using quantile regression. *Proc. 7th. Int. Symp. Geotechnical Safety and Risk*, pp. 188-193.

Westfall, P.H. (2014). Kurtosis as Peakedness, 1905-2014. R.I.P. *The American Statistician*, 68(3) pp. 191-195, https://www.ncbi.nlm.nih.gov/pmc/articles/PMC4321753/.

Zhao, T., Xu, L. & Wang, Y. (2020). Fast non-parametric simulation of 2D multilayer cone penetrometer test (CPT) data without pre-stratification using Markov Chain Monte Carlo simulation. *Engineering Geology*, 273 (2020) 105670, https://doi.org/10.1016/j.enggeo.2020.105670.